Impact of cation compositions on the performance of thin-film transistors with amorphous indium gallium zinc oxide grown through atomic layer deposition

Min Hoe Cho, Min Jae Kim, Hyunjoo Seul, Pil Sang Yun, Jong Uk Bae, Kwon-Shik Park & Jae Kyeong Jeong

Taylor & Francis
Taylor & Francis Group

Impact of cation compositions on the performance of thin-film transistors with amorphous indium gallium zinc oxide grown through atomic layer deposition

Min Hoe Cho[a], Min Jae Kim[a], Hyunjoo Seul[a], Pil Sang Yun[b], Jong Uk Bae[b], Kwon-Shik Park[b] and Jae Kyeong Jeong[a]

[a]Department of Electronics and Computer Engineering, Hanyang University, Seoul, Republic of Korea; [b]R&D Center, LG Display Company, Paju-Si, Kyonggi-Do, Republic of Korea

ABSTRACT

This paper reports the effect of the cation composition on the electrical properties of amorphous indium gallium zinc oxide (*a*-IGZO) thin-film transistors (TFTs) where atomic layer deposition (ALD) was used to deposit an *a*-IGZO channel layer. The $In_{0.38}Ga_{0.18}Zn_{0.44}O$ transistors at a 200°C annealing temperature exhibited 39.4 cm^2/V·s field effect mobility (μ_{FE}), −0.12 V threshold voltage (V_{TH}), 0.40 V/decade subthreshold gate swing (SS), and $> 10^7$ $I_{ON/OFF}$ ratio, corresponding to the state-of-the-art characteristics of transistors with a sputtered IGZO channel. Further enhancement of the μ_{FE} value was observed for the devices with a higher In fraction: the $In_{0.45}Ga_{0.15}Zn_{0.40}O$ transistor had a higher μ_{FE} value of 48.3 cm^2/V·s, −4.06 V V_{TH}, 0.45 V/decade SS, and $> 10^7$ $I_{ON/OFF}$ ratio. The cation composition dependence on the performance of the *a*-IGZO TFTs was explained by analysing the density-of-state (DOS) distribution for the corresponding devices using the experimental independent variable (IV) and theoretical Technology Computer-aided Design (TCAD) simulation.

1. Introduction

The demand for thin-film transistors (TFTs) with high performance has been increasing due to the need for low power consumption, ultra-high pixel density, good form factor, and interactive functionality. In particular, the research on metal oxide semiconductors that are applicable to high-end active-matrix displays is in the spotlight because of their merits, including high mobility, good uniformity over large areas, low process temperature, optical transparency, and cost-effective fabrication process[1–3]. Metal oxides consisting of ternary or quaternary metal compounds (e.g. InZnO, ZnSnO, InGaZnO) have been investigated for use in TFTs, and their electrical properties can be adjusted by varying the relative atomic ratios of the metal ions[4–5]. Among them, amorphous indium gallium zinc oxide (*a*-IGZO) has become an industry-standard channel layer due to its extremely low leakage current, good subthreshold gate swing (SS), reasonable mobility, and good long-term reliability.

Magnetron sputtering is currently mainly used for depositing the *a*-IGZO channel layer because it allows a low-temperature process and good productivity of a facile *a*-IGZO film with a cation composition close to that of the sputtering target material. It is difficult, however, to control the cation composition in the *a*-IGZO film. Also, the presence of high-energy radicals in the plasma chamber can damage the dielectric/semiconductor interface and the growing film itself, which may act as unwanted electrical trap states. Solution-based deposition processes have been developed as alternatives to reduce the fabrication cost of *a*-IGZO films. The device performance and electrical reliability of solution-based oxide transistors, however, have turned out to be inferior to those of sputtering-based devices. Atomic layer deposition (ALD) has gained attention of late as an advanced process for growing an *a*-IGZO channel layer because of its intriguing features, such as its accurate thickness/cation composition controllability, good uniformity, and good step coverage. Some of the previous reports showed better electrical performance compared to the sputtering and solution-based process[6–10].

In this work, TFTs with an *a*-IGZO channel layer grown via ALD were examined. In particular, the cation composition of the a-IGZO film was tailored by adjusting the subcycle duty and consequence. The *a*-IGZO

TFTs with an optimized cation composition exhibited a high field effect mobility (μ_{FE}) of 48.3 cm^2/Vs, −4.06 V threshold voltage (V_{TH}), 0.45 V/decade SS, and $> 10^7$ $I_{ON/OFF}$ ratio. The cation-composition-dependent performances of the *a*-IGZO TFTs were explained by analyzing the distribution of the density of states (DOS) in a band gap, which were extracted by measuring the temperature-dependent independent variable (IV) characteristics based on the Meyer-Neldel rule (MN rule). Such experimental DOS profiles for the various IGZO TFTs were confirmed via Technology Computer-aided Design (TCAD) simulation.

2. Experiment section

2.1. Materials and device preparation

Bottom-gate, top-contact-structure *a*-IGZO TFTs were fabricated on a p$^+$-Si substrate. A heavily doped, p-type Si wafer was used as the gate electrode, and a thermally oxidized 100-nm-thick SiO_2 layer was used as the gate dielectric. 13-nm-thick *a*-IGZO active layers were deposited in a traveling-wave-type ALD apparatus (CN1 Co., Ltd., South Korea). The proposed source canisters are bypass-type: metal precursors were injected directly into the source line, and 50 standard cubic centimeter per minute (sccm) N_2 gas was used as the carrier gas for the precursor delivery. The N_2 gas flow rate was controlled by a mass flow controller. The canister containing the In precursor was maintained at 80°C to provide sufficient vapor pressure and dose, while the canisters containing the Ga and Zn precursors were kept at room temperature because they have sufficient vapor pressure at room temperature. O_3 was used as a reactant. A 970 sccm O_2-30 sccm N_2 gas mixture was introduced into the O_3 generator, which produces O_3 gas at a 250 g/m^3 concentration. An *a*-IGZO active layer was grown in one cycle, which consists of several sequential steps in a sequence of In_2O_3, ZnO, and Ga_2O_3 subcycles. By adjusting the number of subcycles of each binary metal oxide, *a*-IGZO layers with different cation compositions were obtained. A rather long purge time (10 s for each metal precursor and O_3 purge) was adopted to prevent the mixing of the precursors and the reactant. The substrate temperature was set at 250°C, at which simultaneous self-limiting behaviors of the In_2O_3, Ga_2O_3, and ZnO films in terms of the substrate temperature were observed. The *a*-IGZO active layer was patterned via photolithography and wet etching. After that, post-deposition annealing (PDA) was performed in the air for 1 h, at 200°C, for the *a*-IGZO active layer. An indium tin oxide (ITO) film was deposited as a source/drain (S/D) electrode via DC magnetron sputtering, and was patterned through the lift-off method. The

Table 1. Weight percentages obtained through XRF analysis, and atomic percentages obtained by converting the weight percentages.

Cation components	Sample A		Sample B		Sample C	
	wt. %	at. %	wt. %	at. %	wt. %	at. %
In	50	38	54	42	57	45
Ga	17	18	14	15	14	15
Zn	33	44	32	43	29	40

channel width (W) and length (L) of the *a*-IGZO TFTs were 10 and 50 μm, respectively. The completed devices were subjected to contact annealing in the air for 1 h, at 250°C.

2.2. Characterization

The chemical compositions of the *a*-IGZO films were examined via X-ray fluorescence (XRF; Thermo Scientific) spectroscopy, for which the atomic concentration was calibrated via proton-induced X-ray emission. The weight percentages (wt. %) of the cation compositions obtained via XRF analysis for the *a*-IGZO thin films are summarized in Table 1, where the relative cation percentage (at. %) of each film was calculated by considering its molecular weight. The thicknesses of the In_2O_3, ZnO, Ga_2O_3, and *a*-IGZO films were measured via spectroscopic ellipsometry (SE). The chemical states of the *a*-IGZO films were analyzed via X-ray photoelectron spectroscopy (XPS; SIGMA PROBE, ThermoVG). The back surface region (~ 5 nm) of the *a*-IGZO films was etched via plasma in-situ etching in the XPS chamber to remove the surface contamination. In this study, the O *1s* XP spectra were deconvoluted into three asymmetric Lorentzian–Gaussian peaks with a Shirley background. The net electron density (n_e) and mobility of the *a*-IGZO films were evaluated through Hall effect measurement using the van der Pauw configuration. The electrical characteristics of the *a*-IGZO TFTs were measured in the air, at room temperature, using a Keithley 2636 source meter.

3. Results and discussion

Figure 1 shows the variations in the thicknesses of the In_2O_3, Ga_2O_3, and ZnO thin films as a function of the number of ALD cycles. A linear relationship was observed between the number of ALD cycles and the film thickness, which is expected in the typical ALD process.

Figure 2 shows the representative transfer and output characteristics of the *a*-IGZO TFTs with different cation compositions, which were fabricated through 200°C PDA. The μ_{FE} was calculated from the linear
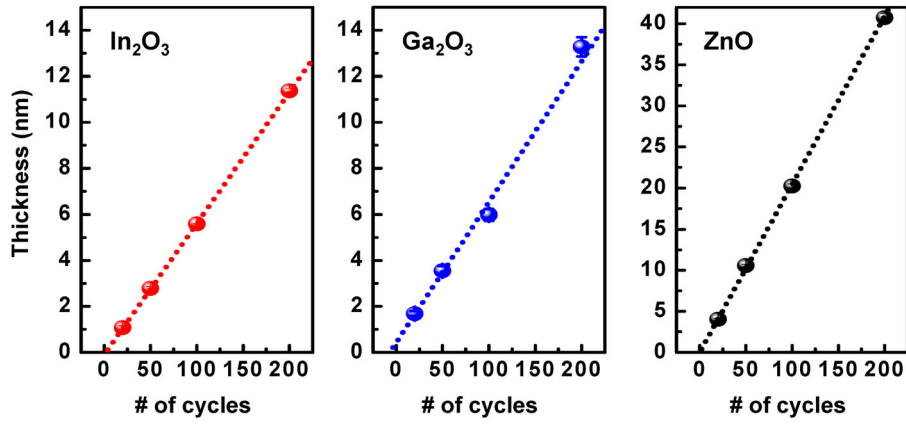
Figure 1. Variations in the thicknesses of the In_2O_3, Ga_2O_3, and ZnO thin films as a function of the number of ALD cycles.
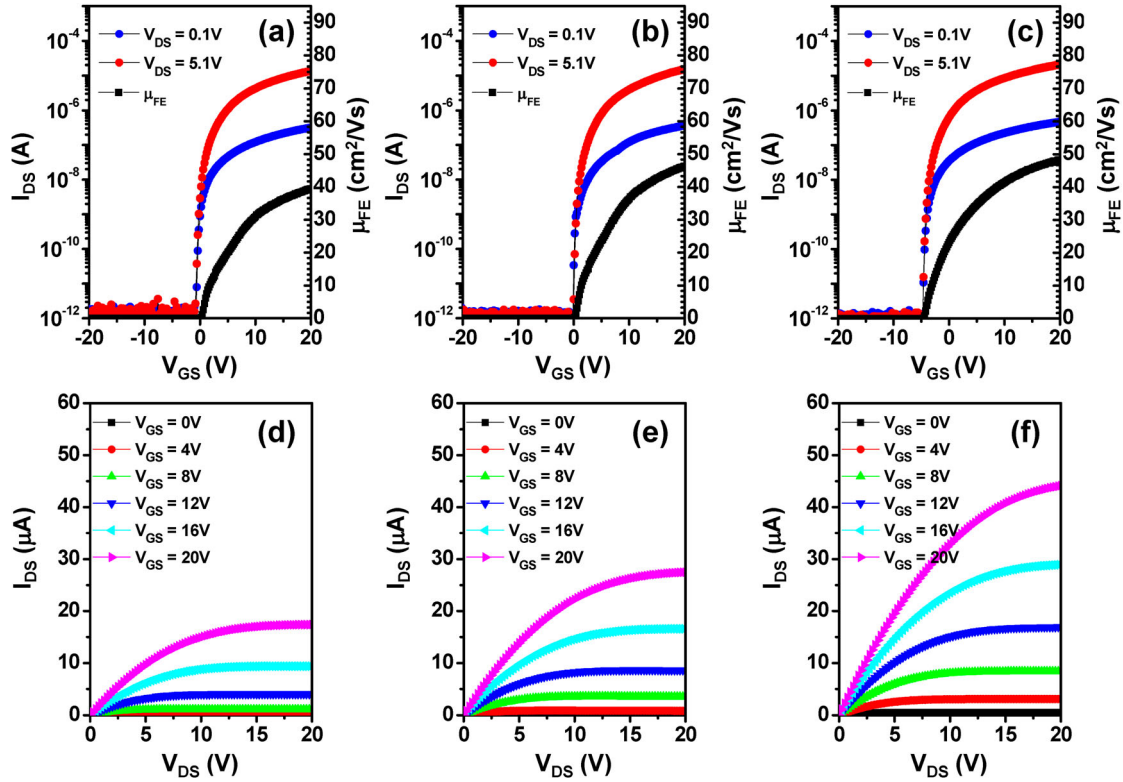

Figure 2. Transfer and output characteristics of the ALD-derived a-IGZO TFT with 200°C PDA: [(a),(d)] In:Ga:Zn $=$ 0.38:0.18:0.44; [(b),(e)] In:Ga:Zn $=$ 0.42:0.15: 0.43; and [(c),(f)] In:Ga:Zn $=$ 0.45:0.15:0.40.

transfer characteristics as $\mu_{FE} = L\cdot g_m/(W\cdot C_{OX}\cdot V_{DS})$ at $V_{DS} = 0.1$ V, where g_m and C_{OX} are the transconductance and oxide capacitance of the gate insulator per unit area, respectively. The μ_{FE} value in this study was extracted at $V_{GS} = 20$ V. The V_{TH} was determined by the gate voltage (V_{GS}), which induces a $L/W \times 10$ nA drain current (I_{DS}) at 5.1 V V_{DS}. The SS ($= dV_{GS}/d\log I_{DS}$ [V/decade]) was extracted from the linear part of the $\log(I_{DS})$ vs. V_{GS} plot. The TFT with an $In_{0.38}Ga_{0.18}Zn_{0.44}O$ channel layer showed a high μ_{FE} value of 39.4 ± 0.6 cm^2/Vs, -0.12 ± 0.13 V V_{TH}, 0.40 ± 0.04 V/decade SS, and $> 10^7$ $I_{ON/OFF}$ ratio

(Figure 2(a) and Table 2). It is noted that these mobility metrics are superior to those of sputtering-based a-IGZO devices. As the In/Ga ratio increased in the IGZO channel layer, the μ_{FE} values of the resulting devices were improved. Thus, the $In_{0.45}Ga_{0.15}Zn_{0.40}O$ transistors exhibited a high μ_{FE} value of 48.3 ± 1.7 cm^2/Vs, -4.06 ± 0.42 V V_{TH}, and 0.46 ± 0.04 V/decade SS without any $I_{ON/OFF}$ ratio ($> 10^7$) compromise. The output characteristics for all the IGZO TFTs showed clear pinch-off, which indicates that the electron transport in the ALD-derived a-IGZO transistor was controlled by the V_{GS} and V_{DS}.

Table 2. μ_{FE}, V_{TH}, SS, and $I_{ON/OFF}$ ratio device parameters of the a-IGZO TFTs with different cation compositions and with 200°C PD**A**.
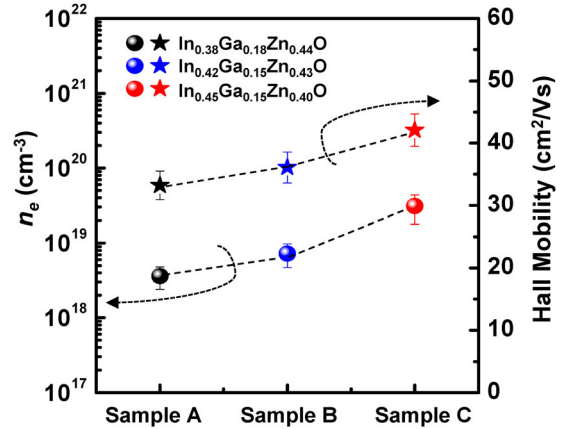
Sample	μ_{FE} [cm^2/Vs]	V_{TH} [V]	SS [V/decade]	$I_{ON/OFF}$
In$_{0.38}$Ga$_{0.18}$Zn$_{0.44}$	39.4 ± 0.6	-0.12 ± 0.13	0.40 ± 0.04	$> 10^7$
In$_{0.42}$Ga$_{0.15}$Zn$_{0.43}$	46.4 ± 1.3	0.57 ± 0.42	0.46 ± 0.04	$> 10^7$
In$_{0.45}$Ga$_{0.15}$Zn$_{0.40}$	48.3 ± 1.7	-4.06 ± 0.42	0.45 ± 0.06	$> 10^7$

Table 3. Deconvoluted O $1s$ peak results of the a-IGZO thin films with different cation composition**s**.

	O $1s$		
Samples	Lattice oxygen (530.5 eV)	Oxygen vacancy (531.5 eV)	Hydroxyl (532.5 eV)
In$_{0.38}$Ga$_{0.18}$Zn$_{0.44}$O	0.57	0.38	0.05
In$_{0.42}$Ga$_{0.15}$Zn$_{0.43}$O	0.54	0.40	0.06
In$_{0.45}$Ga$_{0.15}$Zn$_{0.40}$O	0.52	0.43	0.05

To obtain an insight into the cation-composition-dependent mobility variations for the IGZO TFTs, the chemical states of the a-IGZO films with different cation compositions were examined via XPS. Figure 3 shows the O $1s$ peak XP spectra of the a-IGZO films with different cation compositions. The photoelectron binding energies were calibrated to the C $1s$ peak for the C–C bonds at 284.5 eV. The O $1s$ peak was deconvoluted into three peaks at 530.5, 531.5, and 532.5 eV. The O $1s$ peaks centered at 530.5 and 531.5 eV were assigned to the oxygen in the oxide lattices without and with an oxygen vacancy (V_O), respectively [11]. The peak at 532.5 eV was identified as impurity-related oxygen, such as hydroxyl groups. The relative areas of the V_O-related peak increased monotonically with increasing In/Ga ratio. The values for the In$_{0.38}$Ga$_{0.18}$Zn$_{0.44}$O, In$_{0.42}$Ga$_{0.15}$Zn$_{0.43}$O, and In$_{0.45}$Ga$_{0.15}$Zn$_{0.40}$O films were 38, 40, and 43%, respectively, as summarized in Table 2. On the other hand, the relative areas of the hydroxyl-group-related peaks were nearly independent of the cation composition (Table 3).

Figure 4 shows the variations in the net carrier density (n_e) and Hall mobility estimated from the Hall measurements for the a-IGZO thin films with different cation compositions. The n_e increased with increasing In/Ga ratio in the a-IGZO films. The n_e values for the In$_{0.38}$Ga$_{0.18}$Zn$_{0.44}$O, In$_{0.42}$Ga$_{0.15}$Zn$_{0.43}$O, and In$_{0.45}$Ga$_{0.15}$Zn$_{0.40}$O films were $3.6(\pm1.2) \times 10^{18}$, $7.2(\pm2.5) \times 10^{18}$, and $3.1(\pm1.3) \times 10^{19}$ cm^{-3}, respectively. The corresponding Hall mobility of the IGZO films also increased monotonically with increasing In/Ga ratio. The physical roles of the In cation are well established as those of a mobility enhancer and a carrier generator. First, the intercalation of the In $5s$ orbital in IGZO provides an

Figure 4. Variations in the n_e and Hall mobility of the a-IGZO thin films with different cation compositions extracted via Hall measurement.

effective percolation pathway of electron carriers because its ionic radius is larger than those of the Zn^{2+} and Ga^{3+} ions. Therefore, a higher In loading results in enhanced mobility due to the facile percolation path and the lower effective electron mass. On the other hand, the increasing incorporation of In cation favors the generation of V_O defects as In-O has the lowest bond strength among M-O (M = In, Ga, Zn). The electrical role of the V_O defects depends on the local coordination structure in a-IGZO. A V_O with a large open space or a smaller coordination number, as from a corner sharing site, is calculated to be a shallow or deep trap state, which is frequently observed for the as-deposited or open structure [12]. On the other hand, a V_O with fully coordinated cations, such
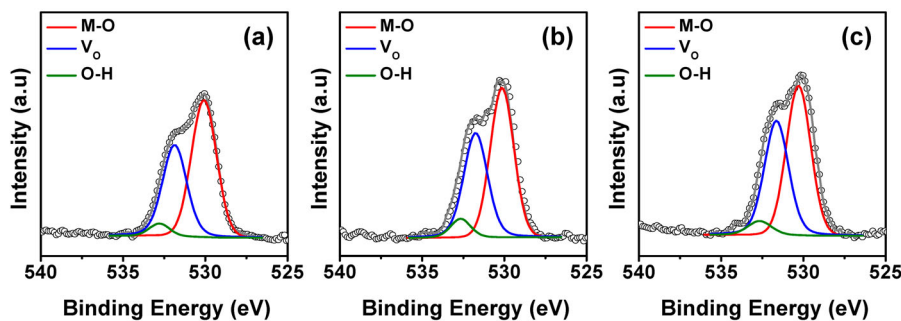
Figure 3. O $1s$ XP spectra of the a-IGZO thin films with different cation compositions: (a) In:Ga:Zn = 0.38:0.18:0.44; (b) In:Ga:Zn = 0.42:0.15:0.43; and (c) In:Ga:Zn = 0.45:0.15: 0.40.

as on a face or an edge of an *a*-IGZO film, acts as a beneficial shallow donor, which is favored in a denser network. Thus, it is obvious that the largest V_O density was obtained for $In_{0.45}Ga_{0.15}Zn_{0.40}O$ (in the O *1s* XP spectra), which is the reason for its highest n_e value (in the Hall effect data). In addition, the highest mobility for the $In_{0.45}Ga_{0.15}Zn_{0.40}O$ TFT can be attributed to not only the smallest percolation path formation but also the percolation-boosting effect based on the proportionality between n_e and μ_{FE} [1].

To obtain an insight into the cation-composition-dependent performance of *a*-IGZO TFTs, the DOS profiles in a forbidden band gap of the *a*-IGZO semiconductor were extracted from the measurement-temperature-dependent IV characteristics based on the MN rule. There are many previous studies that extracted the DOS of the metal oxide TFT by applying the MN rule [13,14]. Following the MN theory, for a thermally activated process (A), a prefactor A_0 can be defined in the following Arrhenius equation:

$$A = A_0 \cdot \exp\left(-\frac{E_A}{kT}\right), \tag{1}$$

where k is the Boltzmann constant, T is the temperature, and E_A is the activation energy of the process. Also, for disordered systems, A_0 and E_A have a correlation that can be described using the following equation:

$$A_0 = A_{00} \cdot \exp\left(\frac{E_A}{E_{MN}}\right), \tag{2}$$

where E_{MN} and A_{00} are the MN energy and prefactor for A_0, respectively. These relationships between A_0 and E_A are observed for the current of conductance in various types of TFTs, whether organic or inorganic. Thus, the thermally activated I_{DS} of the TFTs can be described by the following equations:

$$I_{DS} = I_{DS0} \cdot \exp\left(-\frac{E_A}{kT}\right), \tag{3}$$

$$I_{DS0} = I_{DS00} \cdot \exp\left(\frac{E_A}{E_{MN}}\right), \tag{4}$$

$$I_{DS} = I_{DS00} \cdot \exp\left[\left(\frac{1}{E_{MN}} - \frac{1}{kT}\right)E_A\right], \tag{5}$$

where I_{DS0} and I_{DS00} are the prefactors, respectively, for I_{DS}. From these MN relations, the total DOS distribution for *a*-IGZO TFT devices with different cation compositions with 200°C PDA was calculated. Figure 5(a)-(c)
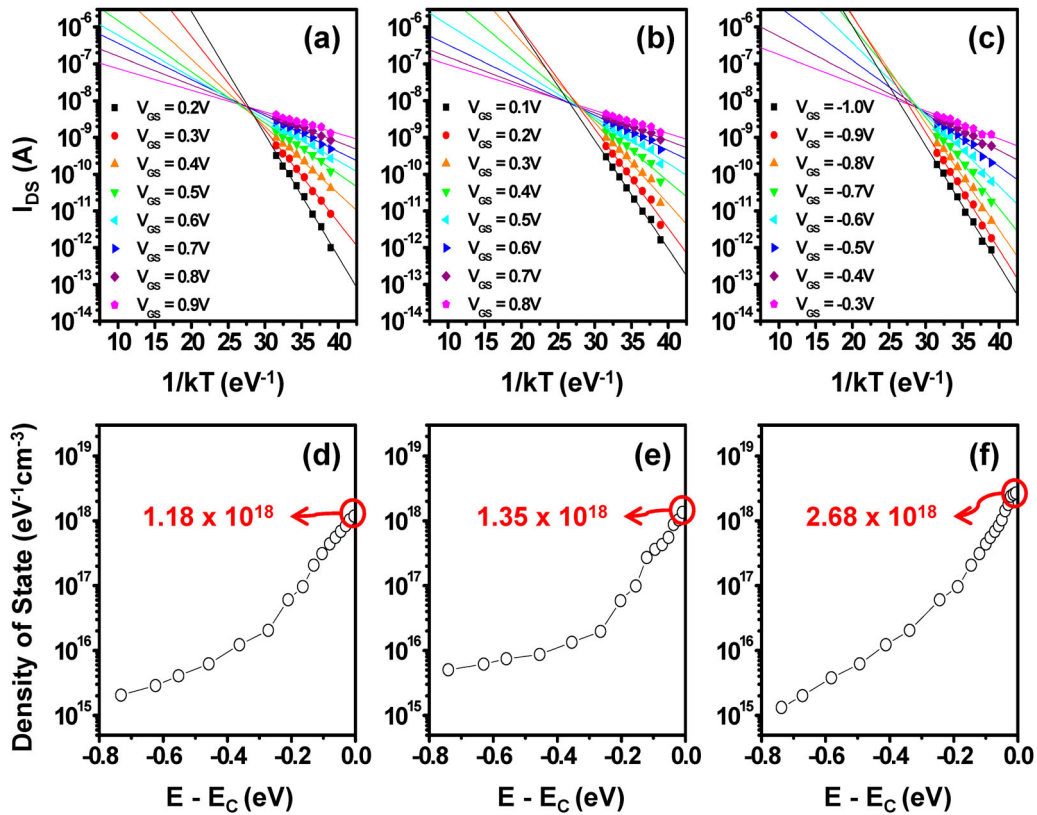

Figure 5. Relationship between 1/*kT* and I_{DS} as a function of V_{GS}, and calculated DOS distribution as a function of the energy (E-E_C) for devices: [(a),(d)] $In_{0.38}Ga_{0.18}Zn_{0.44}O_X$; [(b),(e)] $In_{0.42}Ga_{0.15}Zn_{0.43}O$; and [(c),(f)] $In_{0.45}Ga_{0.15}Zn_{0.40}O$ TFT with 200°C PDA.

show the relationship between $1/kT$ and I_{DS} as a function of V_{GS} for the different a-IGZO TFTs with 200°C PDA, where a common crossing point was clearly observed. For each dataset, E_A and I_{DS0} can be determined using the minimum linear square method. Figure 5(d)-(f) show the calculated DOS distribution as a function of the energy $(E-E_C)$ for the a-IGZO TFTs. The total DOS value at a specific energy level is the summation of N_{it} and N_{SS} because both trap states hinder the moving up of the E_F level at the interface with increasing V_{GS} ($> V_{FB}$). The total DOS distributions were found to increase when the compositions of the In and Ga cations increased and decreased, respectively. A portion of this V_O defect can act as a carrier trap center located in the tailing states below the aforementioned CB edge. This explanation is consistent with the above experimental observation: the increasing DOS distributions with increasing In fraction in the ALD-derived a-IGZO transistors.

TCAD simulation was performed to double-check the MN-rule-based extraction of the DOS distributions of the given a-IGZO TFTs. Figure 6 shows that the measured transfer characteristics of the a-IGZO TFTs can be well fitted by the model obtained from the TCAD simulation incorporating the extracted DOS as a parameter. In the simulation, the free-electron densities $n_{free} = 3.2 \times 10^{17}$, 3.6×10^{17}, and 4.3×10^{17} cm^{-3} for In$_{0.38}$Ga$_{0.18}$Zn$_{0.44}$O, In$_{0.42}$Ga$_{0.15}$Zn$_{0.43}$O, and In$_{0.45}$Ga$_{0.15}$Zn$_{0.40}$O, respectively, and Schottkey barrier height $\Phi_B = 0.26$ eV (between the a-IGZO and S/D ITO electrodes), were used. Figure 7 shows the subgap DOS distribution of the a-IGZO TFTs with different cation compositions obtained from the MN rule and the TCAD simulation. The extracted acceptor-like DOS g(E) close to E_C was empirically modeled to be a superposition of deep and tail states in exponential form, as follows:

$$g(E) = N_{TA} * \exp\left[\frac{E - Ec}{kT_{TA}}\right] + N_{DA} * \exp\left[\frac{E - Ec}{kT_{DA}}\right],$$ (6)

with $N_{TA} = 1.18 \times 10^{18}$, 1.35×10^{18}, and 2.68×10^{18} cm^{-3}, respectively, and $kT_{TA} = 0.06, 0.055$, and 0.05 eV, for the tail states from the conduction band. Also,
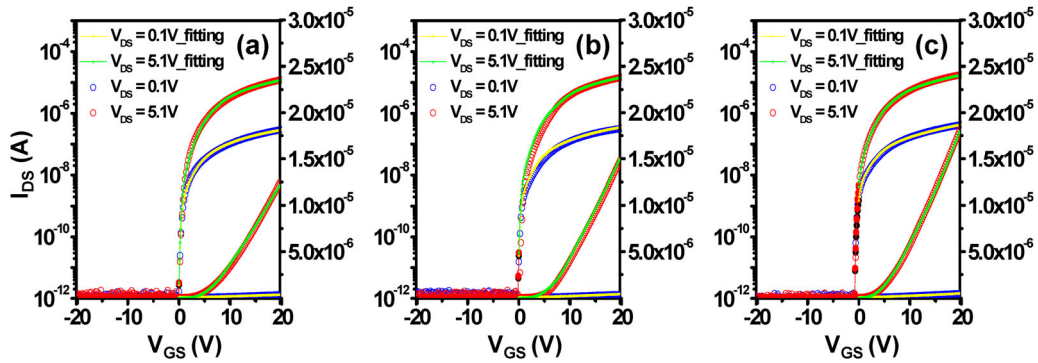

Figure 6. Measured transfer characteristics of the a-IGZO TFTs compared with those of the model obtained from the TCAD simulation incorporating the extracted DOS: (a) In$_{0.38}$Ga$_{0.18}$Zn$_{0.44}$O; (b) In$_{0.42}$Ga$_{0.15}$Zn$_{0.43}$O; and (c) In$_{0.45}$Ga$_{0.15}$Zn$_{0.40}$O TFT with 200°C PDA.
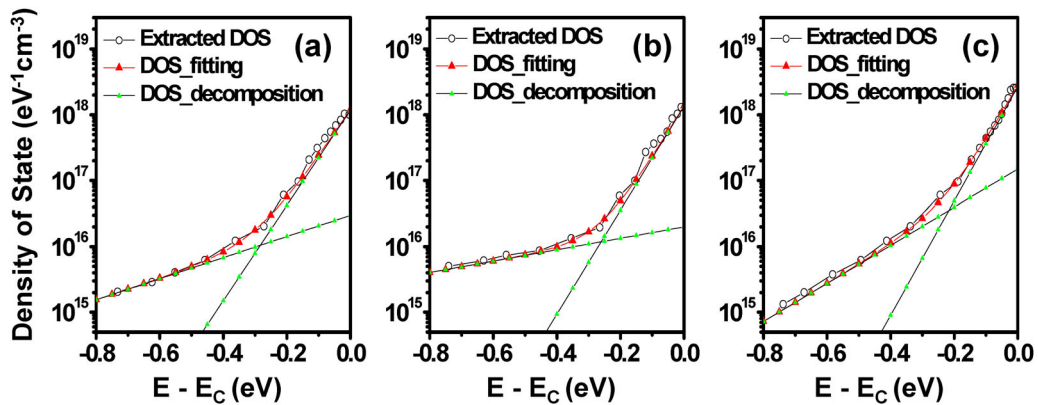

Figure 7. DOS distribution of the a-IGZO TFTs obtained from the MN rule and the comparative result of the TCAD simulation: (a) In$_{0.38}$Ga$_{0.18}$Zn$_{0.44}$O; (b) In$_{0.42}$Ga$_{0.15}$Zn$_{0.43}$O; and (c) In$_{0.45}$Ga$_{0.15}$Zn$_{0.40}$O TFT with 200°C PDA.

$N_{DA} = 3.0 \times 10^{16}$, 2.0×10^{16}, and $1.5 \times 10^{17}\,\mathrm{cm}^{-3}$, respectively, and $k\mathrm{T}_{DA} = 0.27$, 0.50, and 0.15 eV, for the deep states from the conduction band. The comparative result from the TCAD simulation is the well-fitted result of the data obtained from the MN rule.

Finally, it was noted that the gate bias thermal stability of ALD-derived IGZO TFTs is important for their implementation in commercial products. This reliability is being investigated, and the result of the investigation will be reported elsewhere.

4. Conclusion

In this work, the effect of the cation composition on the performance of amorphous indium gallium zinc oxide (*a*-IGZO) thin-film transistors (TFTs) where an IGZO channel layer had been deposited via atomic layer deposition (ALD) was investigated. The cation composition ratio of the *a*-IGZO channel layer was controlled by the changing number of injection subcycles of binary In_2O_3, Ga_2O_3, and ZnO during ALD growth. It was found that the carrier mobility of the fabricated transistors increased with increasing In fraction in the *a*-IGZO film. At the same time, the V_{TH} value showed a negative displacement with increasing In fraction whereas the $I_{ON/OFF}$ ratio was maintained irrespective of the In fraction. This behavior can be well explained by the role of In cation as a carrier generator and an oxygen vacancy (V_O) creator. Thus, the $In_{0.45}Ga_{0.15}Zn_{0.40}O$ transistor exhibited a respectable high μ_{FE} value of 48.3 cm^2/Vs, -4.06 threshold voltage (V_{TH}), 0.45 V/decade subthreshold gate swing (SS), and a good $I_{ON/OFF}$ ratio of $> 10^7$. The Meyer-Neldel rule (MN rule)- and Technology Computer-aided Design (TCAD) simulation-based DOS distribution analysis for the different *a*-IGZO transistors revealed that the acceptor-like tail states below the CB edge increased with increasing In fraction in the *a*-IGZO channel, which is responsible for the higher SS factor for the $In_{0.45}Ga_{0.15}Zn_{0.40}O$ transistor. The high-performance ALD-derived *a*-IGZO semiconductor can be implemented in the various emerging devices for the high-end next-generation active-matrix organic light-emitting diode (AMOLED) and flexible and stretchable display.

Acknowledgement

Funding

Notes on contributors

Min Hoe Cho received his B.S. Materials Science & Engineering degree from Inha University, Incheon, South Korea in 2013. He is currently taking the M.S.-Ph.D. Electronics and Computer Engineering integration course of Hanyang University, Seoul, South Korea. His research interest is the transition metal oxide semiconductor in the device and material aspects, especially the atomic layer deposition process for metal oxide semiconductor devices.

Min Jae Kim received his B.S. Electronic Engineering degree from Hanyang University in 2017. He is currently taking the M.S.-Ph.D. Electronics and Computer Engineering integration course of Hanyang University. His research interest is the high performance and reliability of transition metal oxide semiconductor devices.

Hyeonjoo Seul received her B.S. Materials Science & Engineering degree from Inha University in 2015, and her M.S. Electronic and Computer Engineering degree from Hanyang University in 2017. She is currently enrolled in the Ph.D. Electronics and Computer Engineering course at Hanyang University. Her research interest is the atomic layer deposition process for metal oxide semiconductor devices.

Pil Sang Yun received his B.S. and M.S. Metallurgical Engineering degrees from Korea University, Seoul, South Korea in 2000 and 2002, respectively, and his Ph.D. Material Science degree from Tohoku University, Sendai, Japan in 2012. From 2002 to 2009, he researched on the liquid crystal display (LCD) process and on oxide semiconductor thin-film transistors (TFTs) at AMLCD R&D Center, Samsung Electronics Co., Ltd., South Korea. Since 2012, he has been working at the R&D Center of LG Display Co., Ltd., South Korea, as a senior research engineer. His research has focused on the organic light-emitting diode (OLED) backplane technology using oxide semiconductor TFTs. His research interests are high-performance TFTs and advanced oxide materials with high mobility and reliability, including a novel display process and structure.

Jong Uk Bae received his M.S. Electrical Engineering degree from University of California at Santa Barbara, California, USA, and his Ph.D. degree from University at Buffalo, the State University of New York, Buffalo, New York, USA. He is currently the head of the Fundamental Technology Research Division of the R&D Center of LG Display Co., Ltd., South Korea.

Kwon-Shik Park received his Ph.D. Material Science & Engineering degree from Korea Advanced Institute of Science and Technology (KAIST), South Korea in 1999. Since 2000, he has been with the R&D Center of LG Display Co., Ltd., South Korea, where he has been researching on LCD and OLED device and process technologies as the vice president and the head of the Device Process Research Division. His research has focused on the device technology for advanced displays, the design of integrated circuits based on various backplane technologies, and new materials and processes for future displays.
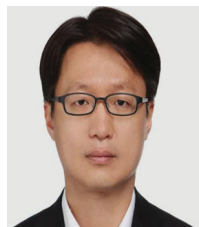
Jae Kyeong Jeong received his B.S., M.S., and Ph.D. Material Science and Engineering degrees from Seoul National University, Seoul, South Korea in 1997, 1999, and 2002, respectively. In 2003, he was a postdoctoral researcher at the University of Illinois at Urbana-Champaign, USA. He joined Samsung Display Corp. as a senior engineer in 2004, where he has performed researches on the design and characterization of low-temperature polysilicon (LTPS) and indium gallium zinc oxide (IGZO) TFTs for the active-matrix organic light-emitting diode (AMOLED) display. In 2009, he joined Inha University as an assistant professor. Since September 2015, he has been a professor at the Department of Electronic Engineering of Hanyang University. He has authored/co-authored more than 140 international journal papers and has 112 international patents.

References

[1] K. Nomura, H. Ohta, A. Takagi, T. Kamiya, M. Hirano, and H. Hosono, Nature 432, 488 (2004).

[2] T. Kamiya, H. Hosono, NPG Asia Mater. 2, 15 (2010).

[3] T. Kamiya, K. Nomura, and H. Hosono, J. Disp. Technol. 5, 273 (2009).

[4] H. Yabuta, M. Sano, K. Abe, T. Aiba, T. Den, H. Kumomi, K. Nomura, T. Kamiya, and H. Hosono, Appl. Phys. Lett. 89, 112123 (2006).

[5] J.I. Kim, K.H. Ji, H.Y. Jung, S.Y. Park, R. Choi, M. Jang, H.-C. Yang, D.H. Kim, J.U. Bae, C.D. Kim, and J.K. Jeong. Appl. Phys. Lett. 99, 122102 (2011).

[6] Y.Y. Lin, C.C. Hsu, M.H. Tseng, J.J. Shyue, and F.Y. Tsai, ACS Appl. Mater. Interfaces 7, 22610 (2015).

[7] P.K. Nayak, Z.W. Wang, D.H. Anjum, M.N. Hedhili, and H.N. Alshareef, Appl. Phys. Lett. 106, 103505 (2015).

[8] A. Illiberi, B. Cobb, A. Sharma, T. Grehl, H. Brongersma, F. Roozeboom, G. Gelinck, and P. Poodt, ACS Appl. Mater. Interfaces **7**, 3671 (2015).

[9] J. Sheng, H.J. Lee, S. Oh, and J.S. Park, ACS Appl. Mater. Interfaces 8, 33821 (2016).

[10] M.H. Cho, H.J. Seol, H.C. Yang, P.S. Yun, J.U. Bae, K.S. Park, and J.K. Jeong, IEEE Electron Device Letters 39, 688 (2018).

[11] G.H. Kim, W.H. Jeong, and H.J. Kim, Phys. Status Solidi A **207**, 1677 (2010).

[12] T. Kamiya, K. Nomura, and H. Hosono, Sci. Technol. Adv. Mater. 11, 044305 (2010).

[13] J.W. Jeong, J.K. Jeong, J.S. Park, Y.G. Mo, and Y.T. Hong, Jpn. J. Appl. Phys. 49, 03CB02 (2010).

[14] K.H. Ji, J.I. Kim, H.Y. Jung, S.Y. Park, Y.G. Mo, J.H. Jeong, J.Y. Kwon, M.K. Ryu, S.Y. Lee, R. Choi, and J.K. Jeong, J. Electrochem. Soc. 157, H983 (2010).